Improved Vectorial Finite-Element BPM Analysis for Transverse Anisotropic Media

José Patrocínio da Silva, Hugo E. Hernández-Figueroa, *Senior Member, IEEE*, and Antonio Manoel Ferreira Frasson

***Abstract*—An efficient finite-element vector beam propagation formulation for dielectric media with transverse anisotropy is thoroughly presented. This formulation is expressed in terms of the magnetic field's transverse components and includes perfectly matched layers at the truncated boundaries and the wide-angle Padé approach. Several key examples demonstrate the usefulness and effectiveness of the present scheme.**

***Index Terms*—Dielectric waveguides, finite elements, optical propagation, transverse anisotropy, vector beam propagation method (BPM).**

I. Introduction

OVER THE LAST decade, a considerable effort has been done to simulate in an efficient and accurate manner the electromagnetic propagation along optical waveguides. One of the most powerful numerical tools used in this field is the beam propagation method (BPM). Among the numerical methods available to discretize the waveguides' cross section, the superior performance achieved when the finite-element method (FEM) is adopted is quite well established by now. So far, a number of scalar, semivectorial, and vectorial finite-element (FE) BPM schemes have been reported in the literature [1]–[3]. For dielectric media, it is quite clear that high accuracy and flexibility is attained by choosing the magnetic field as the wave equation's unknown, due to its continuity over the dielectric interfaces. This permits the use of nodal elements, which exhibit simpler expressions than the edge ones, especially for high order. For this situation, spurious solutions can be efficiently suppressed by forcing the divergence condition into the formulation, which will allow us, as an additional advantage, to eliminate the axial field component. As a consequence, a highly efficient scheme, which solves the magnetic field's transverse components, is obtained. All this has been widely and thoroughly reported in the literature, especially in connection with the so-called modal (eigenvalue) analysis [4], [5]. For the BPM situation, this approach was recently exploited by Obayya *et al.* [3] and Pinheiro *et al.* [6]. In the former, isotropic media was considered, including the perfectly matched layer (PML) and the wide-angle Padé approach; while in the latter, transverse anisotropy was treated, and hard boundary conditions (perfect electric or magnetic walls) and paraxial propagation were adopted.

In [6], the formulation and simplifications adopted make unclear the introduction of the wide-angle approximation. Here, the vector operators are manipulated and presented in such a way that, after a well-accepted simplification, Padé approximants can be straightforwardly introduced.

This paper is organized as follows: In Section II, the FE formulation is presented in detail; the results are shown in Section III, and the conclusions are presented in Section IV. The formulation presented in [6] is reproduced and discussed in the appendix.

II. Formulation

Starting from Maxwell equations, the double-curl Helmholtz equation for the magnetic field $\vec{H}$ is readily obtained as follows:

$$\nabla \times \left(\bar{\bar{k}}\nabla \times \vec{H}\right) - k_0^2\vec{H} = 0 \tag{1}$$

where $\bar{\bar{k}} = 1/\bar{\bar{\varepsilon}}$, with $\bar{\bar{\varepsilon}}$ being the relative permittivity tensor. Considering dielectric media with transverse anisotropy, and defining the unit vectors $\hat{u}_x$, $\hat{u}_y$, and $\hat{u}_z$ associated with x, y, and z directions, respectively, $\bar{\bar{\varepsilon}}$ writes as $\bar{\bar{\varepsilon}} = \bar{\bar{\varepsilon}}_T + \varepsilon_{zz}\hat{u}_z\hat{u}_z$, where $\bar{\bar{\varepsilon}}_T$ is an arbitrary transverse tensor given by $\bar{\bar{\varepsilon}}_T = \varepsilon_{xx}\hat{u}_x\hat{u}_x + \varepsilon_{xy}\hat{u}_x\hat{u}_y + \varepsilon_{yx}\hat{u}_y\hat{u}_x + \varepsilon_{yy}\hat{u}_y\hat{u}_y$. Consequently

$$\bar{\bar{k}} = \bar{\bar{k}}_T + k_{zz}\hat{u}_z\hat{u}_z \tag{2}$$

$$\bar{\bar{k}}_T = \begin{bmatrix} k_{xx} & k_{xy} \\ k_{yx} & k_{yy} \end{bmatrix} = \bar{\bar{\varepsilon}}_T^{-1} \tag{3}$$

$$k_{zz} = \varepsilon_{zz}^{-1}. \tag{4}$$

In addition, k_0 is the free-space wavenumber, and the operator ∇ is defined as

$$\nabla = \hat{u}_x\alpha_x\frac{\partial}{\partial x} + \hat{u}_y\alpha_y\frac{\partial}{\partial y} + \hat{u}_z\alpha_z\frac{\partial}{\partial z} = \nabla_T + \hat{u}_z\alpha_z\frac{\partial}{\partial z} \tag{5}$$

where α_x, α_y, and α_z, are parameters linked to the PML or virtual lossy media. Since the waves are assumed to propagate along the z direction, the parameter α_z is set to unity, while the other PML parameters have to be determined in such a way that the wave impedance is continuous across the interfaces formed between the inner computational domain and the PML. This ensures perfect wave matching over such interfaces, allowing the undesired radiation to leave the effective computational domain freely without any reflection. Following [7] and [8], the PML parameters are specified from the parameter S given by $S = 1 - j(3c/2\omega_0 nd)(\rho/d)^2\ln(1/R)$, where ω_0 is the angular frequency, d is the thickness of the PML, n is the refraction index of the adjacent medium, ρ is the distance from

Manuscript received March 29, 2002; revised October 4, 2002. This work was supported in part by the Brazilian Agency CAPES, CNPq (Project No 301209/94-4) .

The authors are with the Department of Microwaves and Optics, School of Electrical and Computer Engineering, University of Campinas (UNICAMP), 13083-970 Campinas São Paulo, Brazil (e-mail: patroc@dmo.fee.unicamp.br; hugo@dmo.fee.unicamp.br; frasson@dmo.fee.unicamp.br).

Digital Object Identifier 10.1109/JLT.2003.808760

TABLE I
VALUES OF α_x AND α_y

α_x	α_y	PML's location
S	1	Normal to x direction
1	S	Normal to y direction
S	S	On a corner

inner PML's interface, R is the reflection coefficient, and c is the free-space speed of light. Table I describes the parameters α_x and α_y.

For regions outside the PML, i.e., inside the inner or effective computational domain, the parameters $\alpha_{x,y}$ are set to unity. Next, the magnetic field's rapid variation is removed by writing $\vec{H}(x,y,z) = \vec{h}(x,y,z)e^{-jk_0 n_0 z}$, where n_0 is the reference effective index, and $\vec{h}(x,y,z) = \vec{h}_T(x,y,z) + \vec{h}_z(x,y,z)$ is the magnetic field's envelope or slow variation portion. Here, $\vec{h}_T = h_x\hat{u}_x + h_y\hat{u}_y$ and $\vec{h}_z = h_z\hat{u}_z$ represent the magnetic fields' (slow) transverse and axial components, respectively. Using, in addition, the magnetic field divergence condition $\nabla \cdot \vec{H} = 0$, which produces

$$h_z = \frac{\nabla_T \cdot \vec{h}_T + \frac{\partial h_z}{\partial z}}{\gamma} \tag{6}$$

where $\gamma = jk_0 n_0$, after some algebraic manipulations, the axial field can be effectively eliminated from (1), obtaining the following vectorial wave equation, in terms of the (slow) transverse component

$$\begin{aligned} &\overline{\overline{k}}_a \frac{\partial^2 \vec{h}_T}{\partial z^2} - 2\gamma \overline{\overline{k}}_a \frac{\partial \vec{h}_T}{\partial z} - \overline{\overline{k}}_b \nabla_T \left(\nabla_T \cdot \vec{h}_T\right) \\ &\quad - \nabla_T \times k_{zz} \nabla_T \times \vec{h}_T + \left(\overline{\overline{k}}_c + \gamma^2 \overline{\overline{k}}_a\right) \vec{h}_T \\ &\quad + \frac{\partial \overline{\overline{k}}_a}{\partial z}\frac{\partial \vec{h}_T}{\partial z} + \gamma^{-1} \frac{\partial \overline{\overline{k}}_a}{\partial z} \nabla_T \frac{\partial h_z}{\partial z} = 0. \end{aligned} \tag{7}$$

The transverse tensors in (7) are defined as

$$\overline{\overline{k}}_a = \begin{bmatrix} k_{yy} & -k_{yx} \\ -k_{xy} & k_{xx} \end{bmatrix} \tag{8a}$$

$$\overline{\overline{k}}_b = \gamma^{-1} \frac{\partial \overline{\overline{k}}_a}{\partial z} - \overline{\overline{k}}_a \tag{8b}$$

$$\overline{\overline{k}}_c = k_0^2 - \gamma^{-1} \frac{\partial \overline{\overline{k}}_a}{\partial z}. \tag{8c}$$

Following the main BPM's hypothesis, i.e., that the media and fields vary very slowly along the propagation coordinate, we may assume that

$$\left\| \frac{\partial \overline{\overline{k}}_a}{\partial z} \right\| \ll \left| \frac{\partial \vec{h}_T}{\partial z} \right| \ll \left| \frac{\partial \vec{h}_z}{\partial z} \right|. \tag{9}$$

From (9), it becomes clear that the last two terms of (7) are much smaller than the first one, which is supposed to be smaller than the remaining terms of (7). This may be expressed as

$$\left| \frac{\partial \overline{\overline{k}}_a}{\partial z}\frac{\partial \vec{h}_T}{\partial z} + \gamma^{-1} \frac{\partial \overline{\overline{k}}_a}{\partial z} \nabla_T \frac{\partial h_z}{\partial z} \right| \ll \left| \overline{\overline{k}}_a \frac{\partial^2 \vec{h}_T}{\partial z^2} \right|. \tag{10}$$

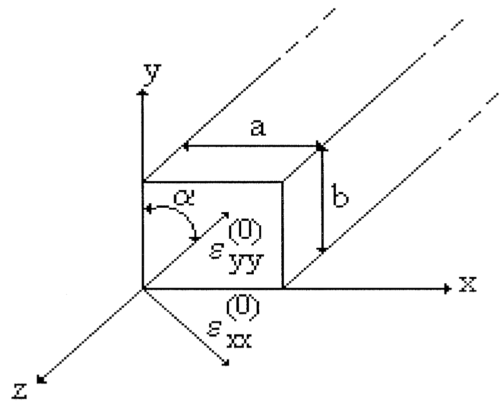

Fig. 1. Anisotropic waveguide optical axes exhibiting an angular displacement α.

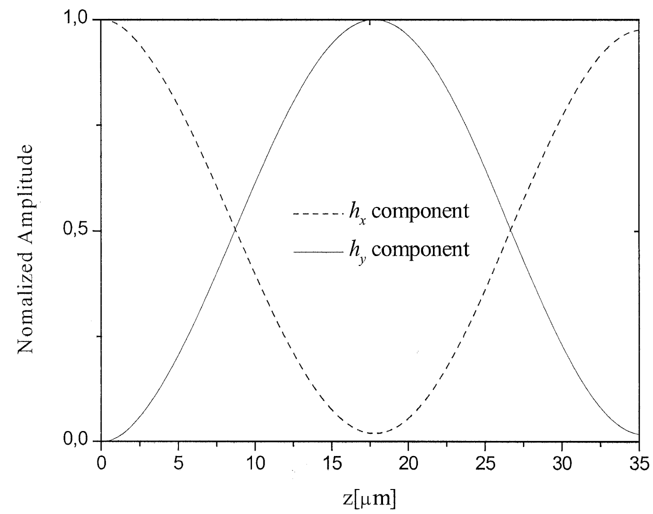

Fig. 2. Variation of h_x's and h_y's normalized amplitudes along the z direction.

Thus, using (10) in (7), the present formulation is obtained and writes as

$$\begin{aligned} &\overline{\overline{k}}_a \frac{\partial^2 \vec{h}_T}{\partial z^2} - 2\gamma \overline{\overline{k}}_a \frac{\partial \vec{h}_T}{\partial z} - \overline{\overline{k}}_b \nabla_T \left(\nabla_T \cdot \vec{h}_T\right) \\ &\quad - \nabla_T \times k_{zz} \nabla_T \times \vec{h}_T + \left(\overline{\overline{k}}_c + \gamma^2 \overline{\overline{k}}_a\right) \vec{h}_T = 0. \end{aligned} \tag{11}$$

The paraxial approximation of (11) is readily obtained by neglecting the first term. The previous formulation given in [6] is reproduced in the appendix [see (49) and (50)]. However, its presentation and interpretation were greatly improved by using the present notation, as can be observed by comparing (49) and (50) with the expressions in [6]. It becomes clear that (50) is structurally different from its paraxial counterpart obtained from (11); moreover, the effective introduction of Padé approximants in (50), taking into account (49), is not quite transparent, as it is in (11) [see (35) and (36)]. This drawback in fact motivated the present work.

Next, applying the conventional FEM to the transverse variation of (11), the cross-sectional domain Ω is divided in Nel triangles, producing Np unknowns over the corresponding nodes. Introducing a set of basis functions (Lagrangian polynomials of

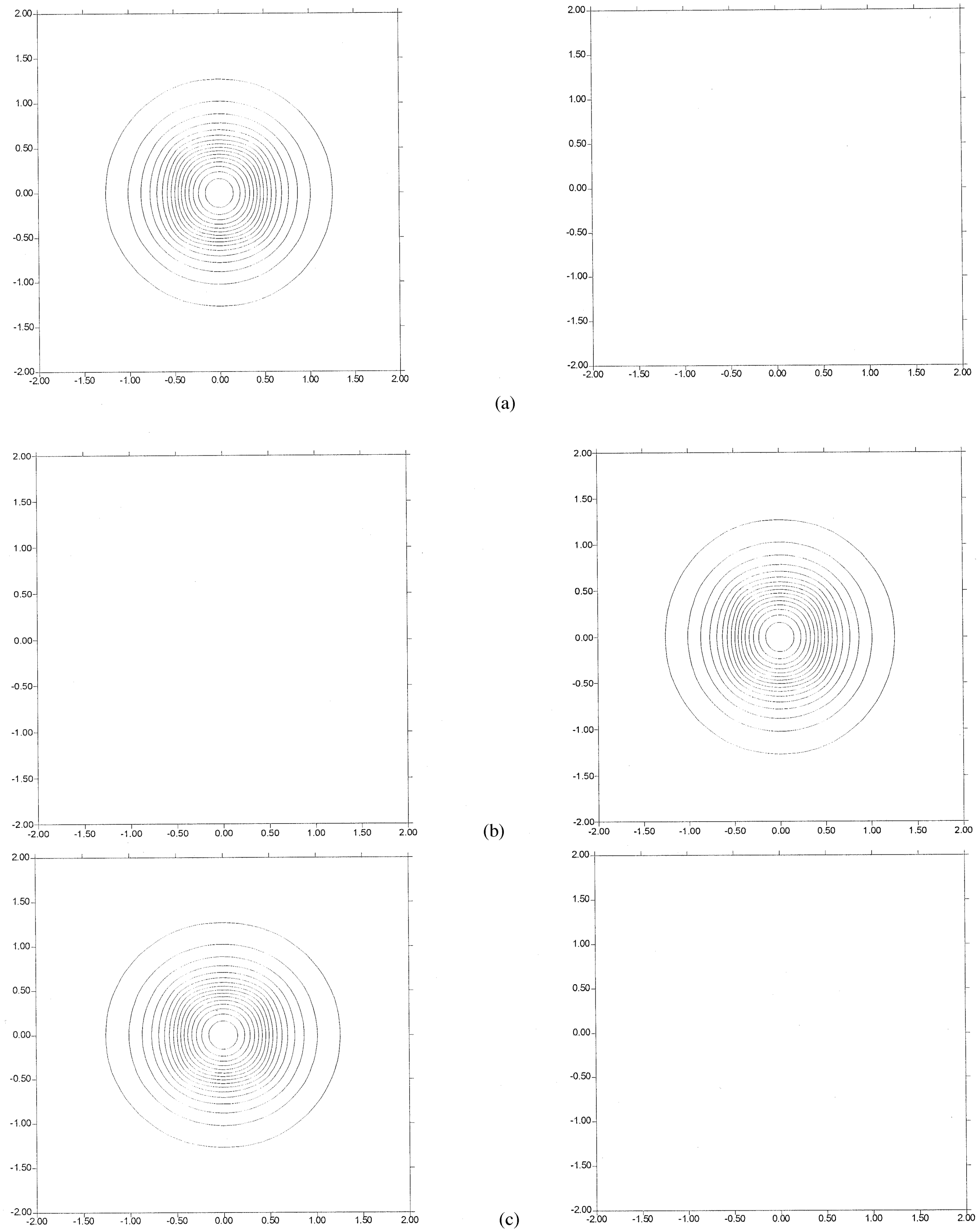

Fig. 3. Modulus of h_x (left column) and modulus of h_y (right column) at (a) $z = 0$ μm, (b) $z = 17.5$ μm, and (c) $z = 35$ μm.

first or second order) $\{\psi\}$, $j = 1, \ldots,$ and Np, then $\vec{h}_T(x, y, z)$ is expressed as

$$\vec{h}_T(x,y,z) = \sum_{j=1}^{Npx} h_{xj}(z)\psi_j(x,y)\hat{u}_x + \sum_{j=Npx+1}^{Np} h_{yj}(z)\psi_j(x,y)\hat{u}_y \quad (12)$$

where the coefficients h_{xj} and h_{yj} represent the unknown field values on the partition's nodes. This expansion, which defines the so-called FE discretization process, leads to the matrix problem

$$[M]\frac{\partial^2\{\vec{h}_T\}}{\partial z^2} - 2\gamma[M]\frac{\partial\{\vec{h}_T\}}{\partial z} + ([K] + \gamma^2[M])\{\vec{h}_T\} = \{0\} \quad (13)$$

where $\{\vec{h}_T\}$ represents a column vector containing the unknowns h_{xj} and h_{yj}, $\{0\}$ is the null column vector, and $[M]$ and $[K]$ are the so-called global matrices, defined by

$$[M]_{ij} = \int_\Omega \overline{\overline{k}}_a \vec{\psi}_j \cdot \vec{\psi}_i d\Omega \quad (14)$$

and

$$
\begin{aligned}
[K]_{ij} = &- \int_{\Omega} \left(k_{zz} \nabla_T \times \vec{\psi}_j \right) \cdot \left(\nabla_T \times \vec{\psi}_i \right) d\Omega \\
&+ \int_{\Omega} \left(\nabla_T \times \vec{\psi}_j \right) \nabla_T \cdot \left(\overline{\overline{k}}_b^{\tau} \vec{\psi}_i \right) d\Omega \\
&- \oint_{\partial\Omega} \left(\nabla_T \cdot \vec{\psi}_j \right) \left(\overline{\overline{k}}_b^{\tau} \vec{\psi}_i \right) \cdot \hat{n} d\ell \\
&+ \int_{\Omega} \overline{\overline{k}}_c \vec{\psi}_j \cdot \vec{\psi}_i d\Omega.
\end{aligned} \tag{15}
$$

Here, $()^{\tau}$ denotes the transpose operation, and

$$\vec{\psi}_j = \psi_j \hat{u} \tag{16}$$

$$\hat{u} = \hat{u}_x, \text{ for } j = 1, \ldots, Npx \tag{17}$$

$$\hat{u} = \hat{u}_y, \text{ for } j = Npx + 1, \ldots, Np. \tag{18}$$

In (14) and (15), $\partial\Omega$ represents all boundaries over the cross-sectional domain Ω, and $\hat{n}$ is the outward normal unit vector linked to those boundaries. Namely, $\partial\Omega$ includes all interfaces $(\partial\Omega_{\text{interf}})$ and the external boundary $(\partial\Omega_{\text{ext}})$. The latter corresponds to the truncated boundary, assumed here to be of rectangular shape, which separates the PML and the infinitely extended region. Since all radiation is supposed to be absorbed inside the PML, $\partial\Omega_{\text{ext}}$ can be chosen to be a perfect electric conductor (PEC) or perfect magnetic conductor (PMC). Here, we choose the former. As observed in previous publications [4], [5], the line integral in (14) vanishes over PEC walls but not over interfaces, where the media exhibits step discontinuity. Therefore, here, such line integral needs to be computed only over $\partial\Omega_{\text{interf}}$. Matrices $[M]$ and $[K]$ can also be expressed as a summation of element matrices linked to the x and y coordinates, over all elements e, as follows:

$$[M] = \sum^{e} \begin{bmatrix} [M_{xx}^e] & [M_{xy}^e] \\ [M_{yx}^e] & [M_{yy}^e] \end{bmatrix} \tag{19}$$

$$[K] = \sum^{e} \begin{bmatrix} [K_{xx}^e] & [K_{xy}^e] \\ [K_{yx}^e] & [K_{yy}^e] \end{bmatrix}. \tag{20}$$

These element matrices can be readily obtained by particularizing the global expressions (14) and (15) over an element e of the partition. They are written as

$$[M_{xx}^e] = k_{yy}^e [S_1^e] \tag{21}$$

$$[M_{xy}^e] = - k_{yx}^e [S_1^e] \tag{22}$$

$$[M_{yx}^e] = - k_{xy}^e [S_1^e] \tag{23}$$

$$[M_{yy}^e] = k_{xx}^e [S_1^e] \tag{24}$$

$$
\begin{aligned}
[K_{xx}^e] = &- k_{zz}^e \alpha_y^2 [S_3^e] - \alpha_x^2 k_{bxx}^e [S_2^e] \\
&- \alpha_x \alpha_y k_{bxy}^e [S_4^e] \\
&- \alpha_x \left(k_{bxx}^e n_x^e + k_{bxy}^e n_y^e \right) [L_1^e] \\
&+ k_{cxx}^e [S_1^e]
\end{aligned} \tag{25}
$$

$$
\begin{aligned}
[K_{xy}^e] = &- k_{zz}^e \alpha_x \alpha_y [S_4^e] - \alpha_y \alpha_x k_{bxx}^e [S_4^e]^{\tau} \\
&- \alpha_y^2 k_{bxy}^e [S_3^e] \\
&- \alpha_y \left(k_{bxx}^e n_x^e + k_{bxy}^e n_y \right) [L_2^e] \\
&+ k_{cxy}^e [S_1^e]
\end{aligned} \tag{26}
$$

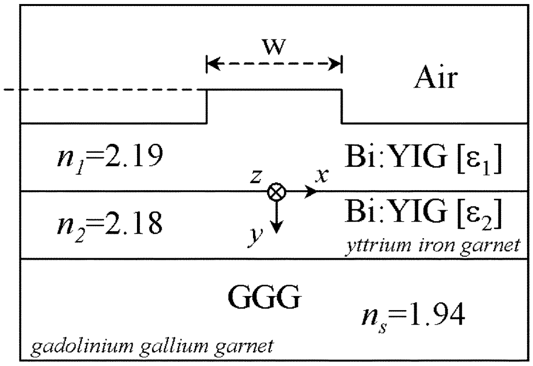

Fig. 4. Magnetooptic optical Isolator.

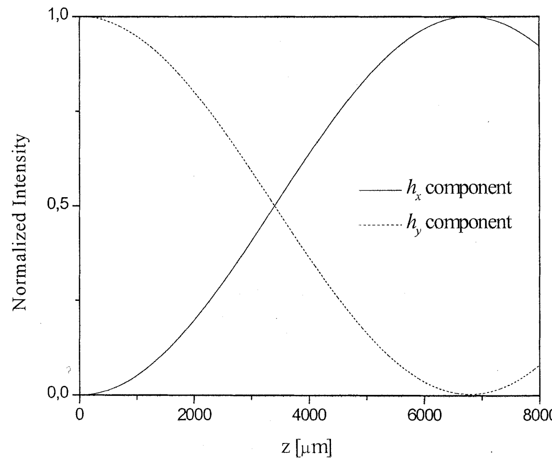

Fig. 5. Normalized intensity variations along z direction.

$$
\begin{aligned}
[K_{yx}^e] = &- k_{zz}^e \alpha_y \alpha_x [S_4^e]^{\tau} - \alpha_x^2 k_{byx}^e [S_2^e] \\
&- \alpha_x \alpha_y k_{byy}^e [S_4^e] \\
&- \alpha_x \left(k_{byx}^e n_x^e + k_{byy}^e n_y^e \right) [L_1^e] \\
&+ k_{cyx}^e [S_1^e]
\end{aligned} \tag{27}
$$

$$
\begin{aligned}
[K_{yy}^e] = &- k_{zz}^e \alpha_x^2 [S_2^e] - \alpha_y \alpha_x k_{byx}^e [S_4^e]^{\tau} \\
&- \alpha_y^2 k_{byy}^e [S_3^e] \\
&- \alpha_y \left(k_{byx}^e n_x^e + k_{byy}^e n_y^e \right) [L_2^e] \\
&+ k_{cyy}^e [S_1^e].
\end{aligned} \tag{28}
$$

Here, k_{zz}^e, k_{rs}^e, and k_{lrs}^e denote, respectively, the average value of components k_{zz}, k_{rs}, and k_{lrs} over the element e. Considering that subindexes (r, s) represent the coordinate pair (x, y), and sub-index l represents b or c, those components are linked to the tensors previously defined in (2), (8), and (9). The auxiliary element matrices $[S_{1,2,3,4}^e]$ and $[L_{1,2}^e]$ are given by

$$[S_1^e] = \int_{\Omega^e} \{\psi^e\}\{\psi^e\}^{\tau} d\Omega \tag{29}$$

$$[S_2^e] = \int_{\Omega^e} \frac{\partial\{\psi^e\}}{\partial x} \frac{\partial\{\psi^e\}^{\tau}}{dx} d\Omega \tag{30}$$

$$[S_3^e] = \int_{\Omega^e} \frac{\partial\{\psi^e\}}{\partial y} \frac{\partial\{\psi^e\}^{\tau}}{\partial y} d\Omega \tag{31}$$

$$[S_4^e] = \int_{\Omega^e} \frac{\partial\{\psi^e\}}{\partial y} \frac{\partial\{\psi^e\}^{\tau}}{\partial x} d\Omega \tag{32}$$

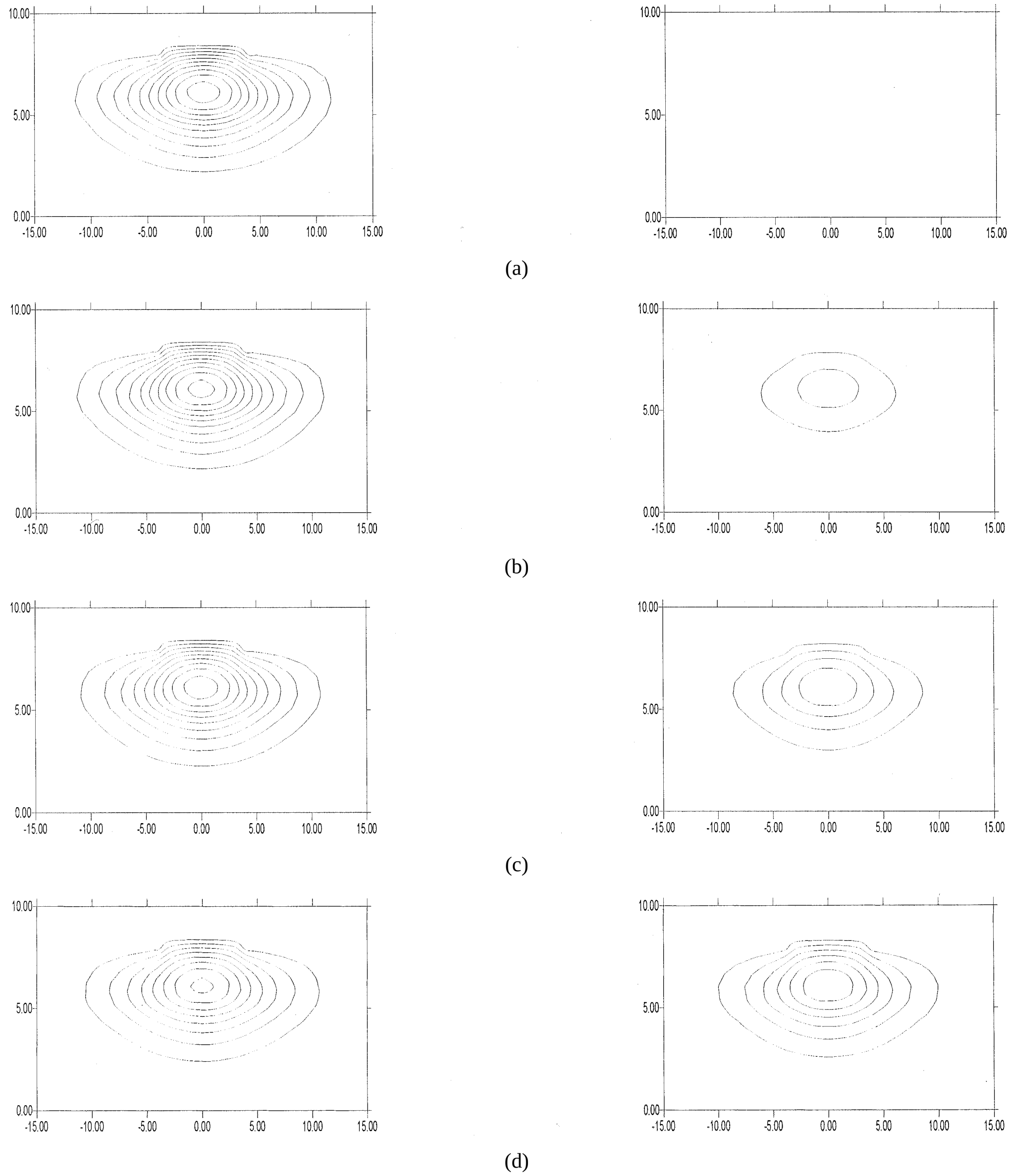

Fig. 6. Modulus of h_y (left side) and h_x (right side) at (a) $z = 0$ μm, (b) $z = 1000$ μm, (c) $z = 2000$ μm, (d) $z = 3000$ μm, (e) $z = 4000$ μm, (f) $z = 5000$ μm, (g) $z = 6000$ μm, and (h) $z = 7000$ μm.

$$[L_1^e] = \oint_{\partial\Omega^e} \{\psi^e\} \frac{\partial\{\psi^e\}^\tau}{\partial x} d\ell \tag{33}$$

$$[L_2^e] = \oint_{\partial\Omega^e} \{\psi^e\} \frac{\partial\{\psi^e\}^\tau}{\partial y} d\ell. \tag{34}$$

Here, $\{\psi^e\}$ represents a column vector containing the corresponding shape functions; Ω^e and $\partial\Omega^e$ denote, respectively, the element e's area and boundary, respectively, and n_x^e and n_y^e are, respectively, the x and y components of the outward normal unit vector linked to $\partial\Omega^e$. Following [8], the Padé (1,1) approximation [9] can be straightforwardly applied to (13), producing the matrix equation

$$[\tilde{M}]\frac{d\{\vec{h}_T\}}{dz} + [K]\{\vec{h}_T\} = \{0\} \tag{35}$$

with

$$[\tilde{M}] = [M] - \frac{1}{4\gamma^2}([K] + \gamma^2[M]). \tag{36}$$

The paraxial equation is easily obtained from (35) by replacing the matrix $\tilde{M}$ by $[M]$. Finally, the θ-finite-difference marching scheme, applied to (35), is written as

$$([\tilde{M}(z)] + \theta\Delta z[K(z)])\{\vec{h}_T(z+\Delta z)\} = ([\tilde{M}(z)] - (1-\theta)\Delta z[K(z)])\{\vec{h}_T(z)\} \tag{37}$$

where Δz is the step's size along the propagation coordinate, and $\theta(0 \leq \theta \leq 1)$ is introduced to control the stability of the method. Extensive tests have shown that stability is ensured when $0.5 \leq \theta \leq 1$. For $\theta = 0.5$, (37) corresponds to the well-known Crank–Nicholson algorithm. However, according to our experience, the best results are obtained for $\theta = 0.55$. This empirical value was adopted for all examples presented in this work. In order to improve the scheme's accuracy, the re-

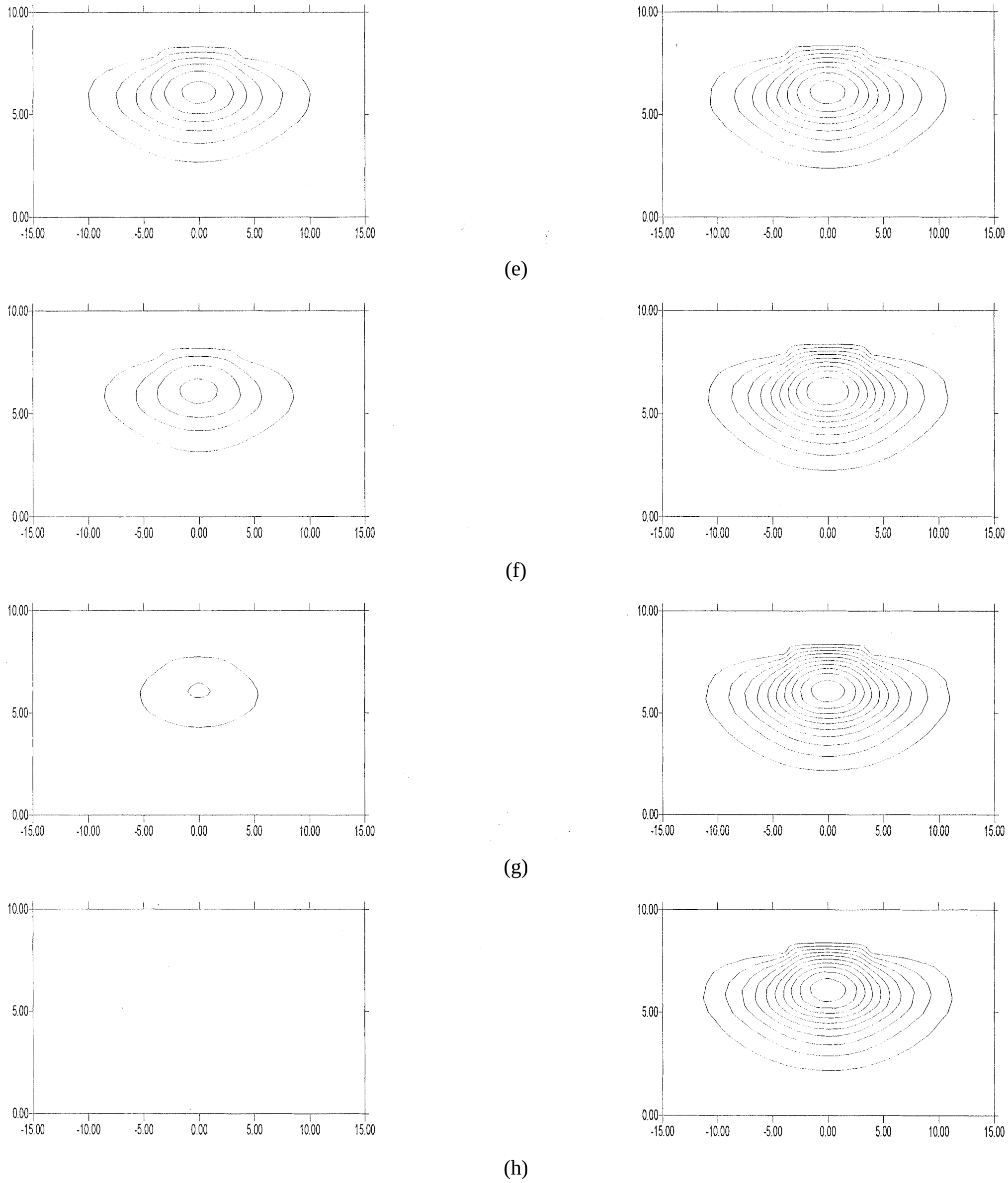

Fig. 6. *(Continued.)* Modulus of h_y (left side) and h_x (right side) at (a) $z = 0\ \mu$m, (b) $z = 1000\ \mu$m, (c) $z = 2000\ \mu$m, (d) $z = 3000\ \mu$m, (e) $z = 4000\ \mu$m, (f) $z = 5000\ \mu$m, (g) $z = 6000\ \mu$m, and (h) $z = 7000\ \mu$m.

fractive index is renewed at each propagation step following the prescription given in [10], as follows:

$$n_0^2(z) = \mathrm{Re}\left[\frac{\{\vec{h}_T(z)\}^\dagger [K(z)]\{\vec{h}_T(z)\}}{k_0^2\{\vec{h}_T(z)\}^\dagger [M(z)]\{\vec{h}_T(z)\}}\right]. \quad (38)$$

Here, † denotes complex conjugate and transpose. Equation (38) can be interpreted as a measurement of the mode spectral composition of $\{\vec{h}_T(z)\}$. Let us call $\{\vec{h}_{T\ell}(z)\}$ and $n_\ell(z)$ the corresponding local modes and local mode effective indexes, respectively, which satisfy the modal eigenvalue problem

$$[K(z)]\{\vec{h}_{T\ell}(z)\} = k_0^2 n_\ell^2(z)[M(z)]\{\vec{h}_{T\ell}(z)\}. \quad (39)$$

By normalizing the local modes

$$\{\vec{h}_{Tm}(z)\}^\dagger [M(z)]\{\vec{h}_{T\ell}(z)\} = \delta_{\ell m} \quad (40)$$

and expanding in terms of the local modes

$$\{\vec{h}_T(z)\} = \sum_{\ell=1}^{Np} \xi_\ell(z)\{\vec{h}_{T\ell}(z)\} \quad (41)$$

(39) is written as

$$n_0^2(z) = \mathrm{Re}\left[\sum_{\ell=1}^{Np} \zeta_\ell(z) n_\ell^2(z)\right] \quad (42)$$

where the positive coefficients $\zeta_\ell(z)$, defined as $\zeta_\ell(z) = |\xi_\ell(z)|^2 / \sum_{m=1}^{Np} |\xi_m(z)|^2$, may be called "mode spectral weights." From (42), the interpretation given for (38) becomes clear. In fact, (42) represents a mode spectral weighted average of the mode effective indexes, linked to the modal composition of $\{\vec{h}_T(z)\}$. Also, using the quantum mechanics jargon, (42) can be viewed as representing the effective index expectation value.

III. Results

To validate our numerical technique we first considered an anisotropic planar waveguide with transverse dimensions a, b as shown in Fig. 1, $a = b = 1$ μm. The channel is embedded in an isotropic dielectric media with index equal to $\sqrt{2.05}$, surrounded by a PML with thickness $d = 1.0$ μm. The channel's ordinary and extraordinary refractive indexes are $\sqrt{2.19}$ and $\sqrt{2.31}$ [11], respectively.

Here, $\varepsilon_{xx}^{(0)}$, $\varepsilon_{yy}^{(0)}$, and $\varepsilon_{zz}^{(0)}$ are the terms of the diagonal tensor ε when the optical axes are aligned with coordinates x and y. In this simulation, we considered a computational window of 8 μm (x direction) $\times$ 8 μm (y direction) covered by 3814 linear elements, while in [11], we used a computational window of 34 μm $\times$ 34 μm covered by 4784 linear elements; the wavelength was $\lambda = 0.86$ μm and $\alpha = 45°$. The permittivity tensor terms are [12]

$$\varepsilon_{xx} = n_o^2 \cos^2\alpha + n_e^2 \sin^2\alpha \tag{43}$$

$$\varepsilon_{yy} = n_e^2 \cos^2\alpha + n_o^2 \sin^2\alpha \tag{44}$$

$$\varepsilon_{zz} = n_o^2 \tag{45}$$

$$\varepsilon_{xy} = \varepsilon_{yx} = \left(n_e^2 - n_o^2\right)\cos\alpha\sin\alpha \tag{46}$$

where α is the rotation angle of the main tensor axes related to the x and y coordinates. The waveguide was excited at $z = 0$ with the fundamental quasi-TM mode E_{11}^x, with $\alpha = 0$, and its corresponding effective propagation constant (β/k_0), obtained using a modal eigenvalue method. Fig. 2 shows the normalized intensity variations of h_x and h_y components for a propagation step of $\Delta z = 0.1$ μm. The switching to a quasi-TE beam occurred at $z = 17.5$ μm, showing perfect agreement with [11].

As we can see in Figs. 2 and 3, the field assumes the initial configuration again at $z = 35$ μm, which is in agreement with the value obtained through the relation $L_B = (\lambda/|\beta_{\text{eff1}} - \beta_{\text{eff2}}|)$ [13], where L_B is the beating length, and β_{eff1} and β_{eff2} are the effective propagation constants of the modes E_{11}^x and E_{11}^y, respectively. Through modal analysis [5], we found $\beta_{\text{eff1}} = 1.473\,934\,94$ and $\beta_{\text{eff2}} = 1.449\,300\,71$; therefore, the beating length was 34.910 767 0 μm, which is in good agreement with the value obtained by the present BPM. Recently, several magnetooptic waveguides have been analyzed in order to obtain very efficient optical isolators. The isolation effect is based on the nonreciprocal behavior of the waveguide with respect to the field propagation direction.

Next, we considered a magnetooptic rib waveguide, as shown in Fig. 4 [14]. The relative permittivity tensor of the Bi:YIG layers is given by

$$[\varepsilon_r] = \begin{bmatrix} \varepsilon_{xx} & j\delta & 0 \\ -j\delta & \varepsilon_{yy} & 0 \\ 0 & 0 & \varepsilon_{zz} \end{bmatrix} \tag{47}$$

where ε_{xx}, ε_{yy}, and ε_{zz} are the permittivity tensor terms in the x, y, and z direction, respectively, and δ represents the first-order magnetooptic effect, which is related to the nonreciprocal Faraday rotation effect.

To analyze this structure, the wavelength used was $\lambda = 1.485$ μm, and the structure parameters are $t_1 = 3.1$ μm, $t_2 = 3.4$ μm, $h = 0.5$ μm, $w = 8.0$ μm, $n_1 = 2.19$, $n_2 = 2.18$, $n_s = 1.94$. Here, θ_f is the Faraday rotation angle given by $\theta_f = k_0\delta/(2n_{\text{eff}})$, with the off-diagonal elements computed assuming $\theta_f = 133°/\text{cm}$, where $n_{\text{eff}} = \beta/k_0$, is the effective refractive index. To simulate this effect, the device geometric birefringence $\Delta_g = 1.1278 \times 10^{-4}$ [5] where $n_{\text{eff}} = 2.184\,017\,54$ and $\delta = 2.396\,413 \times 10^{-4}$ were computed using modal analysis. The magnetooptic permittivities used for the propagation analysis were thus defined as $\varepsilon_{xx1} = \varepsilon_{zz1} = (2.19 - \Delta_g)^2$, $\varepsilon_{yy1} = (2.19)^2$, $\varepsilon_{xx2} = \varepsilon_{zz2} = (2.18 - \Delta_g)^2$, and $\varepsilon_{yy2} = (2.18)^2$. The structure was excited by the y-polarized fundamental mode, obtained through modal analysis. We used a computational window of 30 μm (x direction) $\times$ 30 μm (y direction), covered by 5533 linear elements, and propagation step $\Delta z = 0.1$ μm. By contrast, the computational window needed using the previous paraxial approach [6] was of 200 μm (x direction) $\times$ 100 μm (y direction), covered by 10 365 linear elements. Fig. 5 shows the normalized intensity related to h_x and h_y components, along the propagation direction. Almost perfect mode conversion from the h_y component to the h_x component is achieved at $z = 6700$ μm, in excellent agreement with [1].

Fig. 6, shows the field patterns from $z = 0$ to $z = 7000$ μm, with intervals of 1000 μm. The polarization conversion from h_y to the h_x, along the propagation direction, can be clearly seen.

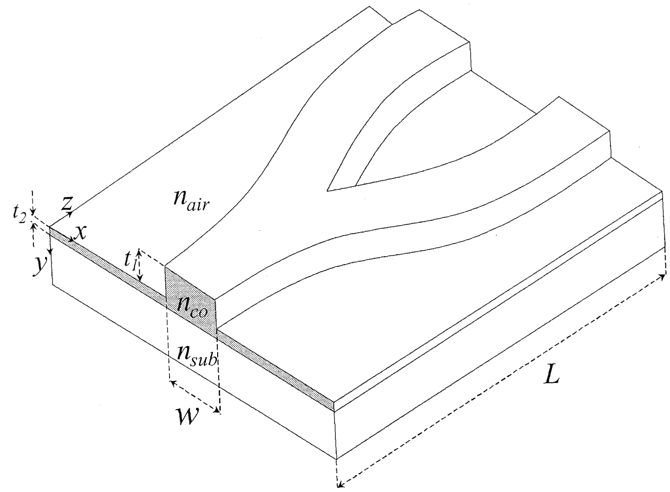

Fig. 7. Rib waveguide Y junction.

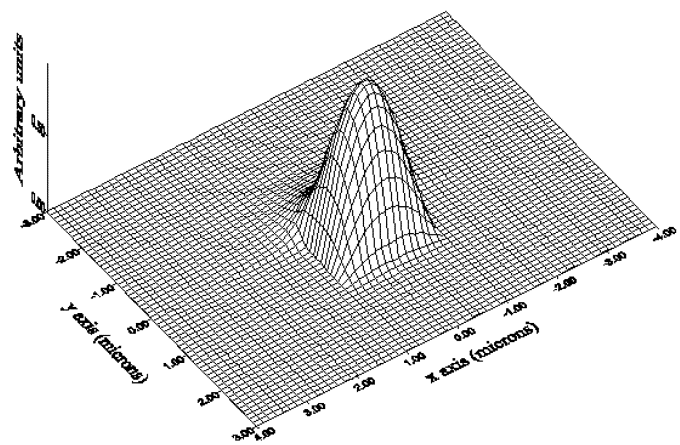

Fig. 8. Fundamental mode's h_y component at $z = 0$ μm.

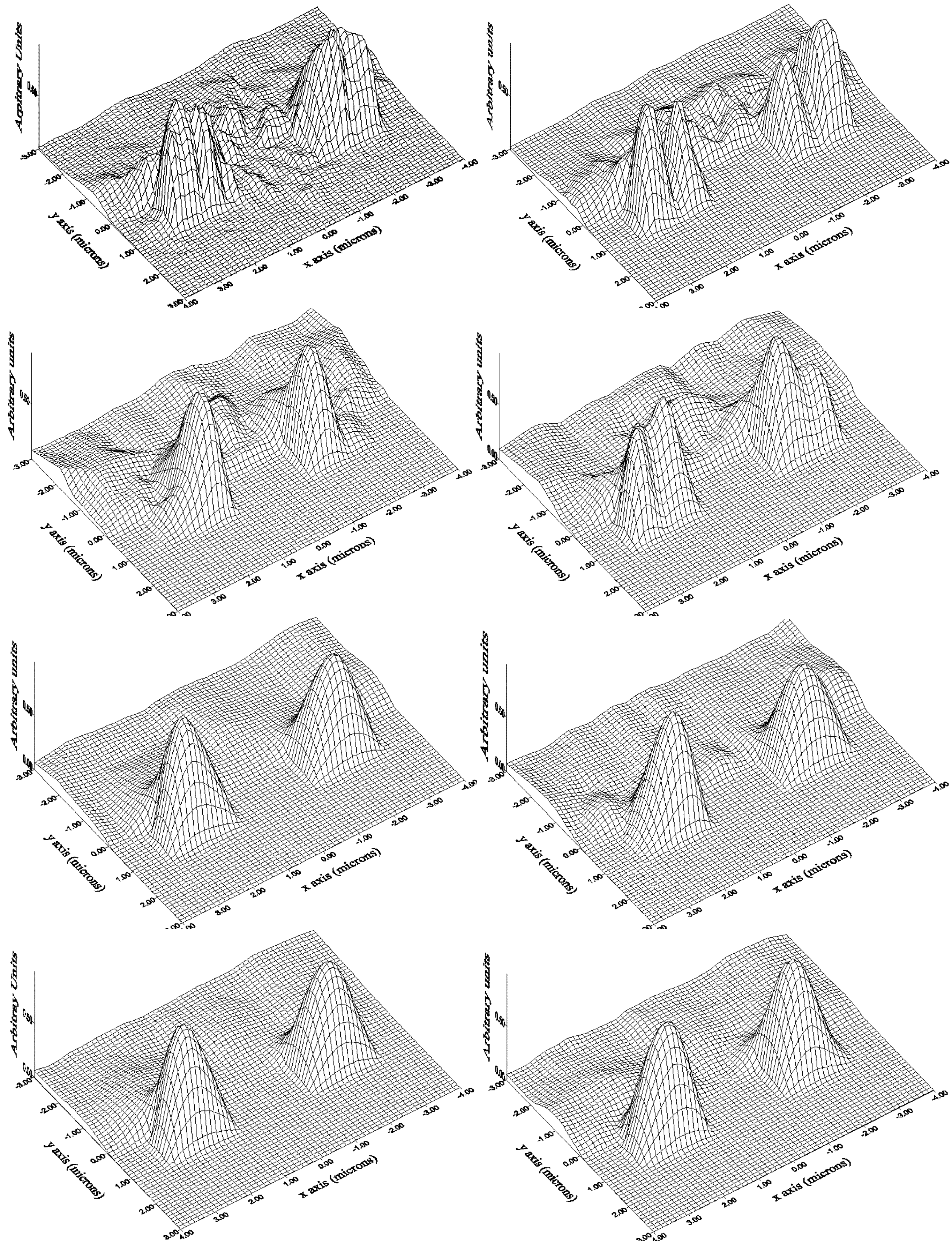

Fig. 9. Variation of the main component of the fundamental mode, plotted from top to bottom. The left column shows the nonparaxial case. The right column shows the paraxial case. (a) $z = 20\ \mu$m, (b) $z = 50\ \mu$m, (c) $z = 175\ \mu$m, and (d) $z = 250$.

Finally, we considered a rib waveguide Y junction as shown in Fig. 7, [16], [17]. This example shows the capability of the new formulation to analyze waveguides varying along the propagation direction and the PML performance. The bifurcation of the waveguide's center follows the curves defined by

$$x = \begin{cases} \pm\left(1 - \cos\left(\frac{\pi z}{L}\right)\right), & z \le L \\ \pm\, 2\ \mu\text{m}, & z > L \end{cases} \tag{48}$$

for $L = 40\ \mu$m. The rib waveguide parameters are $W = 2.0\ \mu$m, $t_1 = 1.1\ \mu$m, and $t_2 = 0.2\ \mu$m, the refractive index of the guiding region is $n_{\rm co} = 3.44$, the substrate refractive index is $n_{\rm sub} = 3.34$, and the refractive index of the medium over of the waveguide is $n_{\rm ar} = 1.0$. The Y junction was excited by the fundamental mode, obtained through modal analysis [5] for $\lambda = 1.55\ \mu$m (see Fig. 8). The PML parameters are given in Table I, the thickness being $d = 1.0\ \mu$m. The computational window used in the previous paraxial formulation [11] was $300 \times 150\ \mu$m and 9516 linear elements. By contrast, here we used a computational window of $12\ \mu$m (x direction) $\times\ 10\ \mu$m (y direction), covered by 4514 linear elements. Fig. 9 shows the comparison between the results obtained by our wide-angle and paraxial schemes, using the same computational window and mesh. As expected, the radiation is treated in a different way by the two approaches.

The wide-angle scheme expels the radiation within a shorter propagation distance than the paraxial one. The results shown in the left column of Fig. 9 are in good agreement with other vector wide-angle BPM schemes reported in the literature [17]. The propagation step was $\Delta z = 0.1\ \mu$m.

IV. Conclusion

A vectorial FE BPM for transverse anisotropic media was presented in detail, which constitutes a substantial improvement on the scheme published in [6]. The present improved scheme is based on a practically new formulation, which permits the insertion of wide-angle approximations in a neat and straightforward manner. Also, PML conditions were included. The present approach's efficiency and usefulness were demonstrated through the analysis of three key examples.

Appendix

Connection With the Previous Formulation

The formulation presented in [6] also started from (1) and made use of the slow variation approximation and the divergence condition (6). Using the present notation, the expression obtained is given by

$$\begin{aligned}
\overline{\overline{k}}_a \frac{\partial^2 \vec{h}_T}{\partial z^2} &- 2\gamma \overline{\overline{k}}_a \frac{\partial \vec{h}_T}{\partial z} - \overline{\overline{k}}_b \nabla_T \left(\nabla_T \cdot \vec{h}_T\right) \\
&- \nabla_T \times k_{zz} \nabla_T \times \vec{h}_T + \left(\overline{\overline{k}}_c + \gamma^2 \overline{\overline{k}}_a\right) \vec{h}_T \\
&+ \frac{\partial \overline{\overline{k}}_a}{\partial z} \frac{\partial \vec{h}_T}{\partial z} + \gamma^{-1} \frac{\partial \overline{\overline{k}}_a}{\partial z} \nabla_T \frac{\partial h_z}{\partial z} \\
&- \gamma^{-1} \overline{\overline{k}}_a \nabla_T \left(\nabla_T \cdot \frac{\partial \vec{h}_T}{\partial z}\right) + \overline{\overline{k}}_a \nabla_T \frac{\partial h_z}{\partial z} \\
&- \gamma^{-1} \overline{\overline{k}}_a \nabla_T \frac{\partial^2 h_z}{\partial z^2} = 0.
\end{aligned} \tag{49}$$

Next, the paraxial approximation reported in [6] was obtained by neglecting the terms containing $\partial^2 \vec{h}_t / \partial z^2$, $\partial^2 h_z / \partial z^2$, and $\partial h_z / \partial z$ and is written as (see [6,(7)])

$$\begin{aligned}
&\left(-2\gamma \overline{\overline{k}}_a + \gamma^{-1} \overline{\overline{k}}_a \nabla_T (\nabla_T \cdot) + \frac{\partial \overline{\overline{k}}_a}{\partial z} \frac{\partial \vec{h}_T}{\partial z}\right) \frac{\partial \vec{h}_T}{\partial z} \\
&\quad - \overline{\overline{k}}_b \nabla_T \left(\nabla_T \cdot \vec{h}_T\right) - \nabla_T \times k_{zz} \nabla_T \times \vec{h}_T \\
&\quad + \left(\overline{\overline{k}}_c + \gamma^2 \overline{\overline{k}}_a\right) \vec{h}_T = 0.
\end{aligned} \tag{50}$$

Though (50) is well defined within the paraxial approach restrictions, as demonstrated in [6], its extension to a Padé (wide-angle) scheme is not straightforward, taking into account the way (49) is presented. On the other hand, our general equation (7) is obtained from (49) by eliminating its last three terms, using (6).

References

[1] Y. Tsuji, M. Koshiba, and N. Takimoto, "Finite element beam propagation method for anisotropic optical waveguides," *J. Lightwave Technol.*, vol. 17, pp. 723–828, Apr. 1999.

[2] P. Liu and B. J. Li, "Semivectorial beam-propagation method for analyzing polarized modes of rib waveguide," *IEEE J. Quantum Electron.*, vol. 28, pp. 778–782, Apr. 1992.

[3] S. S. A. Obayya, B. M. A. Rahman, and H. A. El-Mikati, "New-vectorial numerically efficient propagation algorithm based on the finite element method," *J. Lightwave Technol.*, vol. 18, pp. 409–415, Mar. 2000.

[4] Y. L. Lu and F. A. Fernández, "An efficient finite-element solution for inhomogeneous anisotropic and lossy dielectric waveguides," *IEEE Trans. Microwave Theory Tech.*, vol. 41, pp. 1215–1223, June–July 1993.

[5] H. E. Hernández-Figueroa, F. A. Fernández, Y. Lu, and J. B. Davies, "Vectorial finite element modeling of 2D leaky waveguides," *IEEE Trans. Magn.*, vol. 33, pp. 1710–1713, May 1995.

[6] H. F. Pinheiro and H. E. Hernández-Figueroa, "Novel finite-flement formulation for vectorial beam propagation analysis in anisotropic medium," *IEEE Photon. Technol. Lett.*, vol. 12, pp. 155–157, Feb. 2000.

[7] J. P. Berenger, "A perfectly matched layer for the absorption of electromagnetic waves," *J. Comput. Phys.*, vol. 114, no. 10, pp. 185–200, October 1994.

[8] M. Koshiba, Y. Tsuji, and M. Hikari, "Finite-element beam-propagation method with perfectly mathed layers boundary conditions," *IEEE Trans. Magn.*, vol. 35, pp. 1482–1485, May 1999.

[9] G. R. Hadley, "Wide-angle beam propagation using padé approximation method," *Opt. Lett.*, vol. 17, no. 10, pp. 1426–1428, Oct. 1992.

[10] Y. Tsuji and M. Koshiba, "Adaptive mesh generation for full-vectorial guided-mode and bean-propagation solutions," *IEEE J. Select. Topics Quantum Electron.*, vol. 6, pp. 163–169, Jan./Feb. 2000.

[11] H. F. Pinheiro, "Vectorial beam propagation method based on finite-elements," Ph.D. dissertation, UNICAMP, Sao Paolo, Brazil, 2000.

[12] K. Saitoh and M. Koshiba, "Approximate scalar finite-element beam-propagation method with perfectly matched layers for anisotropic optical waveguides," *J. Lightwave Technol.*, vol. 19, pp. 786–792, May 2001.

[13] H. E. Hernández-Figueroa, "Simple nonparaxial beam propagation scheme for integrated optics," *J. Lightwave Technol.*, vol. 12, pp. 644–649, Apr. 1994.

[14] S. Selleri, L. Vincetti, and M. Zoboli, "Full-vector finite-element beam propagation method for anisotropic device analysis," *J. Quantum Electron.*, vol. 36, pp. 1392–1401, Dec. 2000.

[15] A. Frasson, A. P. Barbero, H. F. Pinheiro, and H. E. Hernandez-Figueroa, "Efficient finite-element analysis of magnetoopitic waveguide," in *Proc. SBMO/IEEE, MTT-S, AP-S and LEOS Int. Micowave Optoelectronics Conf., IMOC*, Rio de Janeiro, Brazil, Aug. 9–12, 1999, pp. 589–592.

[16] Y. Tsuji and M. Koshiba, "Finite element beam propagation method for three-dimensional optical waveguide structures," *J. Lightwave Technol.*, vol. 17, pp. 1728–1734, Feb. 1997.

[17] E. Montanari, S. Selleri, L. Vincetti, and M. Zoboli, "Finite element full-vectorial propagation analysis for three-dimensional z-varying optical waveguide," *J. Lightwave Technol.*, vol. 16, pp. 703–114, Apr. 1998.

José Patrocínio da Silva was born in São João do Sabugí, Rio Grande do Norte, Brazil, on March 6, 1971. He received the Engenheiro Elétrico and the M.Sc. degrees in electrical engineering from the Federal University of Rio Grande do Norte (UFRN), Natal, Brazil, in 1996 and 1999, respectively. Presently, he is working toward the Ph.D. degree at the School of Electrical and Computer Engineering, University of Campinas (UNICAMP), São Paulo, Brazil.

His research includes, computational electromagnetic waves, integrated optics and nonlinear optics.

Hugo E. Hernández-Figueroa (M'94–SM'96) received the Engenheiro Eletrônico degree from the the Federal University of Rio Grande do Sul, Porto Alegre, Brazil, in 1983 and the M.Sc. degree (with thesis) in electrical engineering (antennas and propagation) in 1986, and the M.Sc. degree (with thesis) in applied mathematics and computer science (numerical analysis) in 1988, both from the Pontifical Catholic University of Rio de Janeiro (PUC/RJ), Brazil. He received the Ph.D. degree in physics (optical fibers/integrated optics) from the Imperial College of Science, Technology and Medicine, University of London, London, U.K., in 1992.

From 1984 to 1986, he was a Research Assistant at the Computer Science Department, PUC/RJ. From 1985 to 1989, he was an Assistant Professor at the Military Institute of Engineering, Department of Electrical Engineering, Rio de Janeiro. From 1992 to 1995, he was a Senior Research Fellow at the Department of Electronic and Electrical Engineering, University College London (UCL), University of London. In March 1995, he joined the Department of Microwaves and Optics (DMO), School of Electrical and Computer Engineering (FEEC), UNICAMP, where he is an Associate Professor. From January to March 1998, he was a Visiting Professor at the Department of Electrical and Computer Engineering, University of New Mexico, Albuquerque. Presently, he is the Head of DMO and the leader of the photonics and wireless modeling group (PWMG). He is also a Consultant for several telecommunication companies. He has published over 100 papers in international indexed journals and conferences. His research interests concentrate on a wide variety of modeling and computational aspects of wave electromagnetics based devices and phenomena. He is also involved in research projects dealing with distance learning, virtual labs, multimedia, and web-based technology.

Dr. Hernández-Figueroa was awarded the IEEE Third Millennium Medal in 2000. He is the IEEE MTT-S Representative for Latin America, the President of the IEEE MTT-S and Education Society Chapters linked to the IEEE South Brazil Section, and AdCom Member of the IEEE Education Society. He has served as general chairman and organizer of several international conferences and editor of several special issues in top technical journals. Between 1996 and 1998, he was Vice President of the Brazilian Electromagnetics Society (SBMAG), and between 1998 and 2000, he was Vice President of the Brazilian Microwave and Optoelectronics Society (SBMO).

Antonio Manoel Ferreira Frasson received the B.Sc. degree from the National Telecommunication Institute (INATEL), Santa Rita do Sapucaí, Brazil, in 1984 and the M.Sc. degree from the Telecommunication Studies Center (CETUC), Pontifical Catholic University of Rio de Janeiro, Brazil, in 1989, all in electrical engineering. In 1990, he received the Ph.D. degree in electrical engineering from the University of Campinas (UNICAMP), São Paulo, Brazil, in 2002.

His research interests include computational wave electromagnetics, electromagnetic theory, scattering by complex structures, and microwave circuits.